Superconductivity in the two-dimensional electron gas induced by high-energy optical phonon mode and large polarization of the $SrTiO_3$ substrate

Baruch Rosenstein,[1,2,*] B. Ya. Shapiro,[3,†] I. Shapiro,[3] and Dingping Li[4,5,‡]
[1]*Electrophysics Department, National Chiao Tung University, Hsinchu 30050, Taiwan, R.O.C.*
[2]*Physics Department, Ariel University, Ariel 40700, Israel*
[3]*Physics Department, Bar-Ilan University, 52900 Ramat-Gan, Israel*
[4]*School of Physics, Peking University, Beijing 100871, China*
[5]*Collaborative Innovation Center of Quantum Matter, Beijing, China*
(Received 27 January 2016; revised manuscript received 27 April 2016; published 11 July 2016)

Pairing in one-atomic-layer-thick two-dimensional electron gas (2DEG) by a single flat band of high-energy longitudinal optical phonons is considered. The polar dielectric $SrTiO_3$ (STO) exhibits such an energetic phonon mode and the 2DEG is created both when one unit cell FeSe layer is grown on its (100) surface and on the interface with another dielectric like $LaAlO_3$ (LAO). We obtain a quantitative description of both systems solving the gap equation for T_c for arbitrary Fermi energy ϵ_F, electron-phonon coupling λ, and the phonon frequency Ω, and direct (random-phase approximation) electron-electron repulsion strength α. The focus is on the intermediate region between the adiabatic, $\epsilon_F >> \Omega$, and the nonadiabatic, $\epsilon_F << \Omega$, regimes. The high-temperature superconductivity in single-unit-cell FeSe/STO is possible due to a combination of three factors: high-longitudinal-optical phonon frequency, large electron-phonon coupling $\lambda \sim 0.5$, and huge dielectric constant of the substrate suppression the Coulomb repulsion. It is shown that very low density electron gas in the interfaces is still capable of generating superconductivity of the order of 0.1 K in LAO/STO.

DOI: 10.1103/PhysRevB.94.024505

I. INTRODUCTION

Single layer of iron selenide (FeSe) grown on a strong polar insulator $SrTiO_3$(001) (STO) exhibits superconductivity [1–6] at surprisingly high temperatures (70 K to 100 K). This is an order of magnitude larger than the parent bulk material with the superconducting transition temperature [7] T_c of 8 K. This suggests that the dominant mechanism of creation of the superconductivity in the FeSe layer might differ from that of the bulk FeSe and is caused by influence of the STO substrate. To strengthen this point of view, the high-resolution angle-resolved photoemission spectroscopy (ARPES) experiments [5] and the ultrafast dynamics [3] demonstrated the presence of high-energy phonons in STO. The frequency of the oxygen longitudinal optical (LO) mode reaches $\Omega \approx 100$ meV. In addition, it turns out that the phonons couple strongly to the electrons in the FeSe layer (the coupling constant was estimated to be [3] $\lambda \sim 0.5$, much larger than in the parent material, $\lambda = 0.19$). The band is flat with only a small momentum transfer to electrons. This identification is supported by the earlier ARPES on STO surface states, which shows a phonon-induced hump at approximately 100 meV away from the main band and through inelastic neutron scattering [8]. The role of substrate in assisting superconductivity is not limited to generation of phonons. The polar STO has a huge dielectric constant (estimated to be above $\epsilon = 1000$ on the surface) and hence suppresses Coulomb repulsion inside the FeSe layer.

The nature of electronic states within the FeSe layer is by now quite settled experimentally. The Fermi surface of the single unit cell (1UC) consists of two electron pockets centered around the crystallographic M-point (Brillouin zone corners) with a band bottom below the Fermi level [5] $\epsilon_F = 60$ meV. This means that electrons form a two-dimensional electron gas (2DEG) with small chemical potential. The novelty of the superconducting system is that the occupied states are close to the band edge, very far from the classic case. In both conventional, Bardeen–Cooper–Schrieffer (BCS) and unconventional superconductors the chemical potential is the largest energy scale in the problem (even in quasi-2D high-T_c cuprates the chemical potential is an order of magnitude higher). The scanning tunneling microscope (STM) experiment [6] indicates that the order parameter is gapped (hence no nodes) and, in addition, the quasiparticle interference pattern due to magnetic and nonmagnetic impurities demonstrates that there is no sign change of the order parameter between the two electron pockets. Hence the in -plane order parameter has the s-wave symmetry across the Fermi surface like conventional superconductors (s_{++} in notations adopted for pnictides [9])

An early theory [10] focused on the screening due to the STO ferroelectric phonons on antiferromagnetic spin fluctuations mediated Cooper pairing in parent material FeSe. It suggested that the phonons significantly enhance the Cooper pairing and even might change the pairing symmetry. For the electron-phonon coupling $\lambda \sim 1$ the enhancement was large, although perhaps not enough to explain the experiment. When the interpocket electron-phonon scattering is also strong, opposite-sign pairing will give way to equal-sign pairing. Later [5], it was suggested that the interfacial nature of the coupling assists superconductivity in most channels, including those mediated by spin fluctuations.

Another idea [11] is to use both the electron pockets at the Fermi surface band and the "incipient" hole band below it also found in ARPES, namely generalizing to the multiband model. The conclusion was that "a weak bare

*vortexbar@yahoo.com
†shapib@biu.ac.il
‡lidp@pku.edu.cn

phonon interaction can be used to create a large T_c, even with a spin fluctuation interaction which may be weakened by the incipient band." The difficulty is that the forward scattering nature of the essential phonon processes then means that LO phonons cannot contribute to the interband interaction. Gorkov considered [12] polarization on the surface, screening, and the STO surface LO phonon pairing. His conclusion is that the LO phonon mediated pairing alone cannot account for superconductivity at such high T_c.

The small chemical potential is typical for the STO systems. Another related superconducting (with much lower T_c) 2DEG system with even much smaller chemical potential is the $LaAlO_3$(LAO)-STO interface observed earlier [13]. The microscopic origin of the superconductivity in the LAO/STO system is already quite clear [14]. It is the BCS-like s-wave pairing attributed to the same LO phonon modes discussed above in context of the 1UC FeSe/STO system. Spin fluctuations seem not to play any role in the pairing leading to superconductivity. The phase diagram of LAO/STO is qualitatively similar to the dome-shaped phase diagram of the cuprate superconductors: In the underdoped region, the critical temperature increases with charge carrier depletion.

The theoretical effort to understand the LAO/STO system [15] has resulted in the realization that the Migdal-Eliashberg theory of superconductivity, valid when the phonon frequencies are much smaller than the electron Fermi energy, should be generalized. This is not the case for polar crystals like STO with sufficiently high optical-phonon frequencies, and, consequently, the dielectric function approach proposed long ago by Kirzhnits [16] and developed in Ref. [17] proved to be useful. It was shown that the plasma excitations are important at larger μ (reduce the electron-phonon coupling) and enable us to explain the nonmonotonic behavior of T_c as function of bias that changes chemical potential.

In this paper we further develop a theory of superconductivity in 1UC FeSe/STO and LAO/STO based on the phononic mechanism, including effects of the screened Coulomb repulsion. In the *first stage*, a simple model of 2DEG with pairing mediated by a dispersionless LO phonons is proposed with Coulomb repulsion assumed to be completely screened by huge polarization of STO ($\epsilon \sim 3000$ in 1UC FeSe/STO). In this case, the gap equations of the Frohlich model can be reduced (without approximations) to an integral equation with one variable only and are solved numerically for arbitrary Fermi energy ϵ_F, phonon frequency Ω, and electron-phonon coupling $\lambda < 1$. An expression for the adiabatic and nonadiabatic limits are derived and results for T_c compare well with experiments on 1UC FeSe/STO. Then, in the *second stage*, we include the random-phase approximation (RPA) screened Coulomb repulsion (for somewhat smaller values of dielectric constants are estimated [18] to be $\epsilon = 186$ on the STO side and $\epsilon = 24$ on the LAO side) and solve a more complicated gap equations numerically (without making use of the Kirzhnits ansatz) for various ϵ_F and Coulomb coupling constant. Both the adiabatic, $\epsilon_F >> \Omega$ (conventional BCS), and the nonadiabatic, $\epsilon_F << \Omega$, cases are considered and compared with the local model studied earlier in the context of Bose-Einstein Condensation (BEC) physics [19–22]. The Coulomb repulsion results in significant reduction or even suppression of superconductivity. A phenomenological model for dependence of ϵ_F and λ on electric field for the LAO/STO is proposed.

The paper is organized as follows. The basic 2DEG phonon superconductivity model is introduced in Sec. II. The general Gaussian approximation for weak electron-phonon interactions and RPA screening is described in Sec. III. The superstrong screening case (neglecting Coulomb repulsion altogether) case is solved Sec. IV. The same calculation is performed using the Kirzhnits approach in Sec. V. The general case including the RPA screened Coulomb repulsion is investigated numerically in Sec. VI. The phenomenology of 1UC FeSe/STO and LAO/STO and comparison with experiments are discussed in Sec. VII followed by the Discussion and Summary. Appendices A and B contain the derivation of Gorkov equations and the 2D RPA neutralizing background contribution, respectively.

II. THE LO PHONON MODEL OF 2D PAIRING

As mentioned above, various STO systems including 1UC FeSe/STO (medium to low density) and interface LAO/STO the (very low density) electron gas appears localized in a plane of width of one unit cell (in FeSe layer or on the STO side, respectively). The Hamiltonian of 2D electron gas contains three parts:

$$H = H_e + H_{\rm ph} + H_{e-{\rm ph}}, \tag{1}$$

where

$$H_e = \int_r \psi_\sigma^\dagger \left(-\frac{\hbar^2 \nabla^2}{2m} - \mu \right) \psi_\sigma + \frac{1}{2} \int_{r,r'} n(r) v(r-r') n(r'), \tag{2}$$

and $\psi_\sigma^\dagger, \psi_\sigma$ are the creation and annihilation operators in 2D, $\mathbf{r} = (x, y)$.

The charge density operator is

$$n(r) = \psi^{\sigma\dagger}(r) \psi^\sigma(r), \tag{3}$$

and μ is the chemical potential (Fermi energy). The electron-electron interactions, not related to the crystalline lattice, are described by potential $v(r)$. The electrostatics on the surface/interface is quite intricate [18], and we approximate it by the Coulomb repulsion:

$$v(r) = \frac{e^2}{\epsilon r}, \tag{4}$$

where ϵ is an effective 2D dielectric constant of the system. As mentioned in the Introduction, the effective dielectric constant is huge in STO at low temperatures due to the ionic movements.

Crystal vibrations in STO are highly energetic. The optical phonon mode [8,14] with frequency near $\Omega = 100$ meV is most probably associated with pairing attractive electron-electron force is the ferroelectric LO that involves the relative displacement of the Ti and O atoms. The high-energy STO oxygen LO phonon band mode is separated from all the other phonon bands by a substantial energy gap [8]. The single branch of the optical phonons described by the bosonic field [23] $\phi(r) = \sum_k \frac{1}{\sqrt{2}} (b_k^\dagger e^{-ikr} + b_k e^{ikr})$. The phonon part of the Hamiltonian therefore is

$$H_{\rm ph} = \frac{1}{2} \int_{r,r'} \phi(r) v_{\rm ph}(r-r') \phi(r'), \tag{5}$$

where the phonon energy density $v_{\rm ph}(r-r')$ for the nearly flat LO band is approximately local:

$$v_{\rm ph}(r) = \hbar\Omega\delta(r). \tag{6}$$

Experiments demonstrated a substantial electron-phonon coupling g. In fact, the collective mode energy is greater or comparable to the width of the electron band. Importantly, the electron-phonon coupling allows only a small momentum transfer to the electron,

$$H_{e-ph} = g\int_r n(r)\phi(r). \tag{7}$$

Despite the simplifications, the model is far from being solvable and standard approximations are applied in the following section to obtain the critical temperature of the superconductor. Various "bare" parameters like effective masses, Ω, and the electron-electron and electron-phonon couplings are renormalized as the interaction effects are accounted for.

III. THE PAIRING EQUATIONS

A. Matsubara action

We use the Matsubara time τ $(0<\tau<\hbar/T)$ formalism [23] with action corresponding to the Hamiltonian Eq. (1) (setting $\hbar=1$), $A[\psi,\phi]=A_e[\psi]+A_{\rm ph}[\phi]+A_{e-{\rm ph}}[\psi,\phi]$,with

$$\begin{aligned} A_e &= \int_{r,\tau}\psi^*_\sigma(r,\tau)D^{-1}\psi_\sigma(r,\tau) \\ &\quad +\frac{1}{2}\int_{r,r',\tau} n(r,\tau)v(r-r')n(r',\tau) \\ A_{\rm ph} &= \frac{1}{2}\int_{r,r',\tau}\phi(r,\tau)d^{-1}\phi(r',\tau); \\ A_{e-ph} &= g\int_{r,\tau} n(r,t)\phi(r,t). \end{aligned} \tag{8}$$

Here the electron Green's function is

$$D^{-1} = \partial_\tau - \frac{\nabla^2}{2m} - \mu, \tag{9}$$

while that of the phonon field is

$$d^{-1} = \left(-\partial_\tau^2+\Omega^2\right)\delta(r-r'). \tag{10}$$

In Fourier space the action reads

$$\begin{aligned} A_e &= \sum_{p\omega}\psi^{\sigma*}_{p\omega}D^{-1}_{p\omega}\psi^\sigma_{p\omega} \\ &\quad +\frac{1}{2}\sum_{p\omega p_1 p_2\omega_1\omega_2} v_p\psi^{\sigma*}_{p_1\omega_1}\psi^\sigma_{p_1-p,\omega_1-\omega}\psi^{\rho*}_{p_2\omega_2}\psi^\rho_{p_2+p,\omega_2+\omega}; \\ A_{\rm ph} &= \frac{1}{2}\sum_{k\omega}\phi^*_{k\omega}d^{-1}_\omega\phi_{k\omega}; A_{e-{\rm ph}} \\ &= g\sum_{pp_1\omega\omega_1}\psi^{\sigma*}_{p_1\omega_1}\psi^\sigma_{p_1-p,\omega_1-\omega}\phi_{p\omega} \end{aligned} \tag{11}$$

with electronic,

$$D^{-1}_{p,\omega} = i\omega+\varepsilon_p;\ \varepsilon_p = p^2/2m-\mu, \tag{12}$$

and optical phonon,

$$d^{-1}_\omega = \frac{\omega^2+\Omega^2}{\Omega^2}, \tag{13}$$

propagators, respectively. The fermionic Matsubara frequencies are $\omega_n=\pi T(2n+1)$, while for bosons $\omega_n=2\pi Tn$ with n being an integer. In 2D

$$v_p = \frac{2\pi e^2}{\epsilon p}. \tag{14}$$

The action can be treated with the standard Gaussian approximation.

B. The pairing equations

The electronic action is obtained by integration of the partition function over the phonon field,

$$Z_e[\psi] = \int_\phi e^{-A[\psi,\phi]} = e^{-A^{\rm eff}_e[\psi]}. \tag{15}$$

The Gaussian integral is

$$\begin{aligned} &A^{\rm eff}_e[\psi] \\ &= \sum_{\omega p}\psi^{\sigma*}_{p\omega}D^{-1}_{p\omega}\psi^\sigma_{p\omega} \\ &\quad +\frac{1}{2}\sum_{\omega\omega_1\omega_2 pp_1p_2} V_{p\omega}\psi^{\sigma*}_{p_1-p,\omega_1-\omega}\psi^\sigma_{p_1\omega_1}\psi^{\rho*}_{p_2\omega_2}\psi^\rho_{p_2-p.\omega_2-\omega}, \end{aligned} \tag{16}$$

where $V_{p\omega}=V^{\rm RPA}_{p\omega}+V^{\rm ph}_\omega$. The part of the effective electron-electron attraction due to phonons is

$$V^{\rm ph}_\omega = -g^2\frac{\Omega^2}{\omega^2+\Omega^2}. \tag{17}$$

To take into account screening, we made the replacement $v_p\to V^{\rm RPA}_{p\omega}$ (the random-phase approximation) in 2D,

$$V^{\rm RPA}_{p\omega} = v_p\left[1+\frac{Nmv_p}{\pi}\left(1-x/\sqrt{x^2+1}\right)\right]^{-1}, \tag{18}$$

where $x=|\omega|/(v_Fp)$ with $v_F^2=2\mu/m$.

Performing the standard Gaussian approximation averaging, see Appendix A, one arrives at the Gorkov equations for the normal,$\langle\psi^{\uparrow I\dagger}_{k\omega}\psi^{\downarrow J}_{q\nu}\rangle=\delta_{\omega-\nu}\delta_{k-q}\delta^{IJ}G_{k\omega}$ $(I,J=1,\ldots,N$ are flavors), and the anomalous, $\langle\psi^{\uparrow I}_{k\omega}\psi^{\downarrow J}_{q\nu}\rangle=\delta_{\omega+\nu}\delta_{k+q}\delta^{IJ}F_{k\omega}$, Greens functions. The result is

$$-\Delta^*_{k\omega}F_{k\omega}+D^{*-1}_{k\omega}G_{k\omega}=1 \tag{19}$$

and

$$\Delta_{k\omega}G_{k\omega} = -D^{-1}_{k\omega}F_{k\omega}, \tag{20}$$

where the gap function is defined by

$$\Delta_{k\omega} = \sum\nolimits_{p_1\omega_1} V_{p_1-k,\omega_1-\omega}F_{p_1\omega_1}. \tag{21}$$

Near the critical point one can neglect higher orders in Δ in Eq. (19), resulting in $G=D^*$. Substituting this into Eq. (20), one gets:

$$\sum\nolimits_{p\nu}\left|D_{p\nu}\right|^2 V_{\mathbf{p}-\mathbf{k},\nu-\omega}\Delta_{p\nu} = -\Delta_{k\omega}. \tag{22}$$

Using the explicit form of the propagator D, Eq. (12), the equation takes a final form:

$$\sum_{\mathbf{p}m} \frac{2NT}{\omega_m^2+\varepsilon_p^2} V_{\mathbf{p}-\mathbf{k},m-n}\Delta_{\mathbf{p}m} = -\Delta_{\mathbf{k}n}. \tag{23}$$

C. Simplification of the integral equations for critical temperature for the s-wave pairing

Transforming to polar coordinates and using rotation invariance, $\Delta_{\mathbf{p}\nu} = \Delta_{p\nu}$, $p = |\mathbf{p}|$, and then changing the variables to $\varepsilon_p = p^2/2m - \mu$, the electronic part of the kernel of Eq. (23) is

$$\int_{\varepsilon_2=-\mu}^{\Lambda-\mu} \frac{mNT}{\pi} \sum_{n_2} \frac{1}{\omega_{n_2}^2+\varepsilon_2^2} P_{\varepsilon_1\varepsilon_2;n_1-n_2}\Delta_{\varepsilon_2 n_2} = -\Delta_{\varepsilon_1 n_1}. \tag{24}$$

Here Λ is an ultraviolet cutoff of the order of atomic energy scale $\hbar^2/2ma^2$ with lattice spacing a. The phonon part of the kernel, $P_{\varepsilon_1,\varepsilon_2,n} = P^{\mathrm{RPA}}_{\varepsilon_1,\varepsilon_2,n} + P^{\mathrm{ph}}_n$, is

$$P^{\mathrm{ph}}_n = -\frac{g^2\Omega^2}{\omega_n^2+\Omega^2}, \tag{25}$$

while in the screened Coulomb part is

$$P^{\mathrm{RPA}}_{\varepsilon_1,\varepsilon_2,n} = \frac{e^2}{\epsilon}\int_{\phi=0}^{2\pi} \left\{ \begin{array}{c} \sqrt{2(s-r\cos\phi)}+ \\ +\frac{2e^2}{\epsilon}\left[1-|\omega_n|/\sqrt{\omega_n^2+4\mu(s-r\cos\phi)}\right] \end{array} \right\}^{-1}. \tag{26}$$

This formula along with the treatment of the neutralizing background is derived in Appendix B. Here we have used abbreviations

$$\begin{aligned} s &= \varepsilon_1+\varepsilon_2+2\mu; \\ r &= 2\sqrt{(\varepsilon_1+\mu)(\varepsilon_2+\mu)}. \end{aligned} \tag{27}$$

To symmetrize the kernel viewed as a matrix, one makes rescaling of the gap function

$$\eta_{\varepsilon n} = \frac{1}{\sqrt{\omega_n^2+\varepsilon^2}}\Delta_{\varepsilon n}, \tag{28}$$

leading to eigenvalue equation

$$\int_{\varepsilon_2=-\mu}^{\Lambda-\mu} \sum_{n_2} K_{\varepsilon_1 n_1;\varepsilon_2 n_2}\eta_{\varepsilon_2 n_2} = \eta_{\varepsilon_1 n_1}, \tag{29}$$

where the symmetric matrix is

$$K_{\varepsilon_1 n_1;\varepsilon_2 n_2} = -\frac{mNT}{\pi}\frac{1}{\sqrt{\omega_{n_1}^2+\varepsilon_1^2}\sqrt{\omega_{n_2}^2+\varepsilon_2^2}} P_{\varepsilon_1\varepsilon_2,n_1-n_2}. \tag{30}$$

Critical temperature is obtained when the largest eigenvalue of the matrix K is the unit. This was done numerically by discretizing variable ε. The numerical results for the full model are presented in Sec. IV; however, since the screening of the STO is very strong, we first neglect the Coulomb repulsion altogether. This allows a significant simplification.

IV. SUPERCONDUCTIVITY IN THE LO PHONON MODEL

In this case, the theory Eqs. (2) and (5) has three parameters (in addition to temperature), the optical phonon frequency Ω, the electron-phonon coupling g, and chemical potential μ. We first relate the bare coupling g to the "binding energy E_c" conventionally determined in the BCS-BEC crossover studies [19,21,22]. Then, since this simplified model will be applied to the 1UC FeSe on STO, one prefers to parametrize the electron gas via carrier density n related to the Fermi energy by $\epsilon_F = \pi\hbar^2 n/m$ instead of chemical potential μ. Following the standard practice, T_c is found by solving the second Gorkov equation [Eq. (22)]. This is compared with a simpler Kirzhnits approach applied to the present case in the next section. To simplify the presentation and without too much loss of generality we take the number of flavors $N = 1$.

A. Binding energy

It is customary [19,22] to relate the electron-phonon coupling g to the energy of the bound state $E_b \equiv 2E_c$ created by this force in quantum mechanics in vacuum (the two-particle sector of the multiparticle Hilbert space). We use the binding energy to estimate the parameter range in which chemical potential μ approaches the Fermi energy ϵ_F defined above. In 2D the threshold scattering matrix element for total energy E at zero momentum obeys the integral Lippmann-Schwinger equation for scattering amplitude:

$$\Gamma(\omega,\nu,2E) = -V^{\mathrm{ph}}_{\omega-\nu} - \frac{1}{2\pi}\int_\rho V^{\mathrm{ph}}_{\omega-\rho} f(\rho,E)\Gamma(\rho,\nu,2E), \tag{31}$$

where

$$\begin{aligned} f(\rho,E) &= \frac{1}{(2\pi)^2}\int_{\mathbf{p}} \frac{1}{p^2/2m+E+i\rho}\frac{1}{p^2/2m+E-i\rho} \\ &= \frac{m}{2\pi}\int_{\varepsilon=E}^{\Lambda}\frac{1}{\varepsilon^2+\rho^2} = \frac{m}{4|\rho|}\left(1-\frac{2}{\pi}\arctan\frac{E}{|\rho|}\right). \end{aligned} \tag{32}$$

The equation Eq. (31) coincides with the sum of "chain diagrams" at zero chemical potential in the many-body theory with Γ being the "renormalized coupling" [24]. The bound state (there is only one such bound state in 2D) with binding energy $2E_c$ is found as a singularity of $\Gamma(\omega,\nu,2E)$. It occurs at an energy for which the matrix of the linear equation (31) has zero eigenvalue, so the eigenvector $\psi(\rho)$ obeys

$$\int_\rho \left[2\pi\delta(\omega-\rho) + V^{\mathrm{ph}}_{\omega-\rho} f(\rho,E_c)\right]\psi(\rho) = 0. \tag{33}$$

Changing the variables, $\psi(\rho) = f(\rho,E)^{-1/2}\eta(\rho)$, this equation can be presented as the unit eigenvalue problem

$$\frac{mg^2}{2\pi}\int_\rho K(\omega,\rho)\eta(\rho) = \eta(\omega), \tag{34}$$

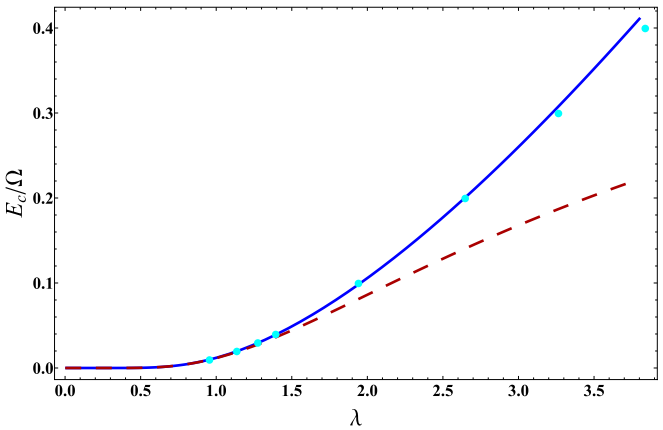

FIG. 1. The 2D binding energy per electron of two electrons in the bound state created by the attraction due to LO dispersionless phonon branch with frequency Ω. The (bare) coupling strength λ is in a wide range, $\lambda \sim 0$–3.5. The essential exact dependence found numerically (dots) is compared with weak coupling (the solid line) and results obtained using the local model (dashed line).

with a symmetric kernel

$$K(\omega,\rho) = \frac{1}{4}\sqrt{\frac{1}{|\omega|}\left(1-\frac{2}{\pi}\arctan\frac{E_c}{|\omega|}\right)}\frac{1}{|\rho|}\left(1-\frac{2}{\pi}\arctan\frac{E_c}{|\rho|}\right) \times \frac{\Omega^2}{(\omega-\rho)^2+\Omega^2}. \tag{35}$$

It turns out that the unit eigenvalue is the maximal eigenvalue of this positive definite matrix. The discretized version of Eq. (34) was diagonalized numerically. The results are presented in Fig. 1.

Solution found numerically is well fitted by

$$\frac{2\pi}{mg^2} = \frac{1}{\lambda} \approx \frac{1}{2}\sinh^{-1}\left[\frac{\Omega(\Omega+\pi E_c)}{\pi E_c(\Omega+E_c)}\right], \tag{36}$$

where the 2D dimensionless electron-phonon coupling (per spin) is defined as $\lambda = \frac{mg^2}{2\pi\hbar^2}$. As will be demonstrated in the following subsections, the interesting range of couplings will obey $\epsilon_F >> E_c$ and thus [22] we always replace μ by ϵ_F.

It has the correct asymptotics at both weak and strong coupling, so

$$\frac{E_c}{\Omega} = \frac{1}{2\sinh\left[\frac{2}{\lambda}\right]}\left\{1-\sinh\left[\frac{2}{\lambda}\right] + \sqrt{\left(1-\sinh\left[\frac{2}{\lambda}\right]\right)^2+\frac{4}{\pi}\sinh\left[\frac{2}{\lambda}\right]}\right\}. \tag{37}$$

At weak coupling,

$$E_c/\Omega = \frac{2}{\pi}e^{-2/\lambda} << 1, \tag{38}$$

and hence one can use a local "instantaneous" electron-phonon interaction model, with Eq. (25) approximated by

$$P_n^{\rm ph} = -\frac{g^2\Omega^2}{\omega_n^2+\Omega^2} \approx -g^2\theta(\Omega-|\omega_n|), \tag{39}$$

to describe this limit. In the instantaneous model the electron-phonon interaction is assumed to vanish on the scale of Ω. In Eq. (42), it is clear that in whole range of parameters of interest the first term is replaced by $\pi/2$. The results for E_c are consistent with the BEC literature [22], see the dashed line in Fig. 1. Note that the dimensionless pre-exponential factor in Eq. (38) is determined to be $\frac{2}{\pi}$ while our notation for Λ does not coincide with the Chubukov notation, which is, in our notation, $\frac{2}{\pi}\Omega$.

B. The energy independence of the gap function

Equation (24) in the limit $e^2 \to 0$ is

$$\frac{g^2mT}{2\pi}\sum_{n_2}\int_{\varepsilon_2=-\epsilon_F}^{\Lambda-\epsilon_F}\frac{1}{\omega_{n_2}^2+\varepsilon_2^2}\frac{\Omega^2}{(\omega_{n_1}-\omega_{n_2})^2+\Omega^2}\Delta_{\varepsilon_2 n_2} = \Delta_{\varepsilon_1 n_1}. \tag{40}$$

Since the left-hand side of the equation is independent of ε_2, the gap function is independent of energy: $\Delta_{\varepsilon n} = \Delta_n$. Substituting this, one gets a one-dimensional integral equation,

$$\lambda T\sum_{n_2}\frac{\Omega^2}{(\omega_{n_1}-\omega_{n_2})^2+\Omega^2}\Delta_{n_2}\int_{\varepsilon_2=-\epsilon_F}^{\Lambda-\epsilon_F}\frac{1}{\omega_{n_2}^2+\varepsilon_2^2} = \lambda\sum_{n_2}\frac{\Omega^2 f(\omega_{n_2})}{(\omega_{n_1}-\omega_{n_2})^2+\Omega^2}\Delta_{n_2} = \Delta_{n_1}, \tag{41}$$

where the integral is

$$f(\omega) = \frac{T}{|\omega|}\left(\arctan\frac{\Lambda-\epsilon_F}{|\omega|}+\arctan\left[\frac{\epsilon_F}{|\omega|}\right]\right). \tag{42}$$

Changing of variables, $\eta_n = \sqrt{f(\omega_n)}\Delta_n$, makes the kernel matrix of the integral equation,

$$\sum_{n_2}K_{n_1n_2}(T)\eta_{n_2} = \eta_{n_1}, \tag{43}$$

symmetric,

$$K_{n_1n_2}(T) = \lambda\frac{\sqrt{f(\omega_{n_1})f(\omega_{n_2})}\Omega^2}{(\omega_{n_1}-\omega_{n_2})^2+\Omega^2}. \tag{44}$$

C. Numerical procedure and results

The eigenvalue equation Eq. (43) is solved numerically by diagonalizing sufficiently large matrix $K_{n_1n_2}(T)$. The index $-N_\omega/2 < n < N_\omega/2$ with the value $N_\omega = 256$ used. At this value of N_ω the results are already independent of the UV cutoff Λ. The critical temperature for given λ, ϵ_F and Ω is determined from the requirement that the largest eigenvalue of $K(T)$ is 1. The results presented as functions of ϵ_F in Fig. 2 in whole range of ϵ_F and Fig. 3 for $\epsilon_F < \Omega$.

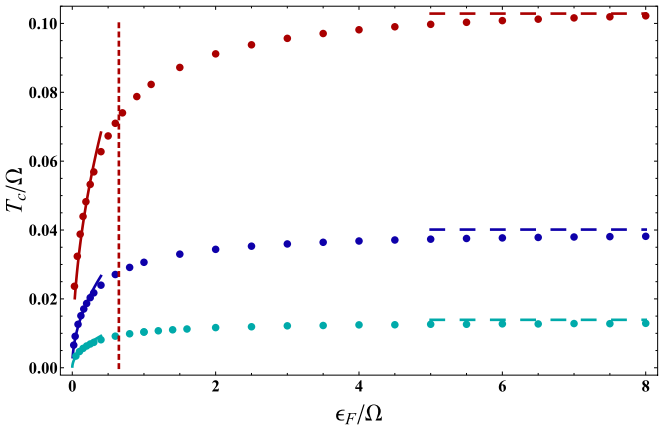

FIG. 2. The critical temperature of a 2DEG-LO phonon superconductor (the Coulomb repulsion is assumed to screened out by the substrate). T_c in units of the phonon frequency Ω is given as a function of the Fermi energy in whale range of ϵ_F/Ω for the dimensionless electron-phonon coupling (from top to bottom): $\lambda = 0.5,0.34,0.25$. The adiabatic (BCS) limit is a dashed line. The solid line is the result of the local theory.

D. Adiabatic and nonadiabatic (local interaction model) limits

In the strongly adiabatic situation, $\epsilon_F >> \Omega$, one can take the $\epsilon_F \to \infty$ limit in which the matrix simplifies, $f(\omega) \approx \frac{\pi T}{|\omega|}$,

$$K^{\rm BCS}_{n_1 n_2}(T) = \frac{\lambda}{\sqrt{|n_1+1/2||n_2+1/2|}\left\{\left[2\pi\frac{T}{\Omega}(n_1-n_2)\right]^2+1\right\}}. \tag{45}$$

This can be fitted by the phenomenological McMillan-like formula (dashed lines in Fig. 2),

$$T_c^{\rm adiab}(\lambda) \approx 0.75\ \Omega \exp\left[-\frac{1}{\lambda}\right]. \tag{46}$$

In the opposite strongly nonadiabatic limit, $E_c << \epsilon_F << \Omega$, the local model defined in subsection A can be used. The gap equation Eq. (41) for frequency independent $\Delta_n = \Delta$ simplifies into

$$\lambda \sum\nolimits_{n_2=-\Omega/(2\pi T_c)}^{\Omega/(2\pi T_c)} f(\omega_{n_2})\Delta = \Delta. \tag{47}$$

The solution exists for

$$\lambda T_c \sum\nolimits_{n=-\Omega/(2\pi T_c)}^{\Omega/(2\pi T_c)} \frac{1}{|\omega_n|}\left(\frac{\pi}{2} + \arctan\left[\frac{\epsilon_F}{|\omega_n|}\right]\right) = 1. \tag{48}$$

At low temperatures the sum can be approximated by an integral

$$\frac{\lambda}{\pi}\int_{\omega=\pi T_c}^{\Omega}\frac{1}{\omega}\left(\frac{\pi}{2} + \arctan\left[\frac{\epsilon_F}{\omega}\right]\right) = 1, \tag{49}$$

one gets the formula

$$T_c^{\rm local}(\lambda) = \sqrt{E_c(\lambda)\epsilon_F} = \sqrt{\frac{2\Omega\epsilon_F}{\pi}}\exp\left[-\frac{1}{\lambda}\right]. \tag{50}$$

The curves are given in Fig. 3 (dashed lines) and compare well with the simulated result (circles) for $\lambda = 0.5,0.34,0.25$ (from top to bottom).

There exists an alternative approach to such calculations (beyond the Gaussian approximation adopted here), see Ref. [20] in which the correlator at zero chemical potential is subtracted. We do not use it, but very recently Chubukov *et al.* found [22] that for the local instantaneous model the results are identical. It is instructive to compare the direct numerical simulation with a simpler approximate semianalytic Kirzhnits method that is applied to the model in the following section.

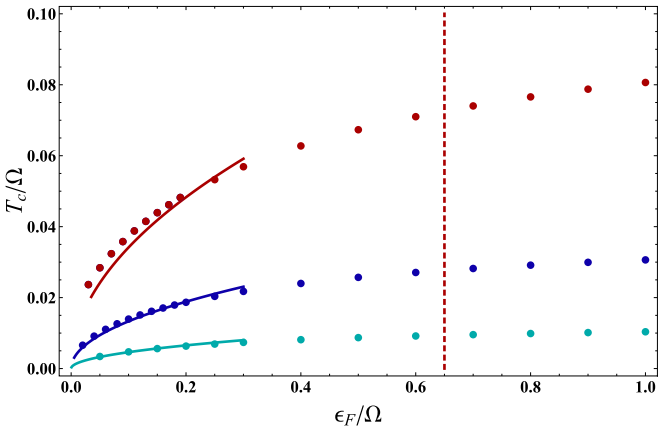

FIG. 3. The critical temperature of a 2DEG-LO phonon superconductor in the low temperatures range in units of the phonon frequency Ω for $\lambda = 0.5,0.34,0.25$. Solid line is the result of the local theory.

V. COMPARISON WITH THE KIRZHNITS ANSATZ

A. Application of the Kirzhnits method to the LO phonon model

Integral equations in general [Eqs. (43)] are very complicated and typically approximated by simpler one-dimensional integral equations. It was first proposed long ago by Kirzhnits [16,17] and later developed for the dielectric function approach to novel superconductors [15]. In this section the units of $\hbar = m = \Omega = 1$ and physical frequency (not Matsubara) are used. Spectral representation of the dispersionless optical phonon contribution to inverse dielectric constant is

$$\sigma(k,E) = \frac{\epsilon}{e^2}\lambda k\delta(1-E^2). \tag{51}$$

The gap equation for the quantity characterizing the anomalous average F_p defined by Kirzhnits [16] reads,

$$\Phi(p) = -\frac{e^2}{2\pi\epsilon}\int_{\mathbf{k}}\frac{B(\varepsilon_k)}{|\mathbf{p}-\mathbf{k}|} \times\left[1-2\int_{E=0}^{\Lambda}\frac{\sigma(|\mathbf{p}-\mathbf{k}|,E)}{E+|\varepsilon_k|+|\varepsilon_p|}\right]\Phi(k), \tag{52}$$

where

$$B(\varepsilon_k) = \frac{\tanh(\varepsilon_k/2T_c)}{2\varepsilon_k}. \tag{53}$$

Substituting Eq. (53) into Eq. (52), and transforming the variable k to the energy, one obtains:

$$\Phi(p) = \lambda\int_{\varepsilon_k=-\epsilon_F}^{\Lambda-\epsilon_F}\frac{B(\varepsilon_k)}{1+|\varepsilon_k|+|\varepsilon_p|}\Phi(k). \tag{54}$$

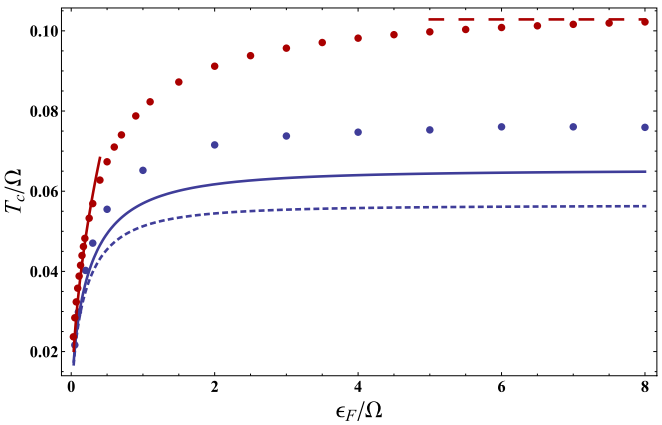

FIG. 4. Comparison with the critical temperature of the Kirzhnits ansatz approximation for a wide range of Fermi energies. The brown dots are the same as in Fig. 2 for $\lambda = 0.5$ while the solid line is the result of the instantaneous (local) theory. The Kirzhnits approximation T_c calculated numerically is given by blue dots, while the dashed and solid blue lines are the weak-coupling approximation analytic results at leading and the next to leading order, respectively.

Symmetrization of the kernel, $\Phi(p) = \sqrt{B(\varepsilon_p)}\eta_p$, one obtains:

$$\lambda \int_{\varepsilon_2=-\epsilon_F}^{\Lambda-\epsilon_F} \frac{\sqrt{B(\varepsilon_1)B(\varepsilon_2)}}{1+|\varepsilon_1|+|\varepsilon_2|}\eta_2 = \eta_1. \tag{55}$$

This is solved numerically for $\epsilon_F = 0.5, 1, 5\Omega$, and $\lambda = 0.5$ with the ultraviolet cutoff $\Lambda = 15\Omega$ in the upper limit of integral in Eq. (55) with number of values of energy $N_\varepsilon = 4000$, so the step is smaller than $(\epsilon_F + \Lambda)/N_\varepsilon \sim 10^{-2}$. The results are presented in Figs. 4 and 5.

It is possible to obtain a closed analytic expression only at weak coupling.

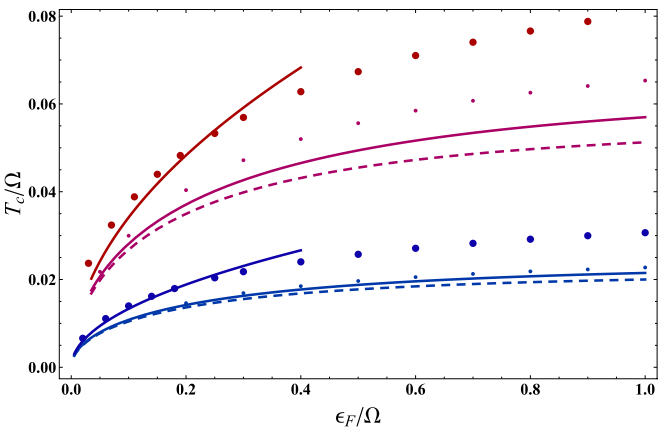

FIG. 5. Comparison with the critical temperature of the Kirzhnits ansatz approximation for a small Fermi energies. The brown dots are the result of numerical solution of the gap equation and are the same as in Fig. 2 for $\lambda = 0.5$ and 0.34, where the solid line is the result of the instantaneous theory. The Kirzhnits approximation T_c, calculated numerically, is given by blue dots, while the dashed and solid blue lines are the weak-coupling approximation analytic results at leading and the next to leading order, respectively.

B. Weak coupling

At small coupling the critical temperature can be estimated analytically using the asymptotic theory from Zubarev [25]:

$$T_c = \frac{2}{\pi} e^{\gamma_E} \epsilon_F e^{-\frac{1}{\lambda}} e^{\zeta(\epsilon_F,\lambda)}, \tag{56}$$

where

$$\zeta(\epsilon_F,\lambda) = \int_{\varepsilon=-\epsilon_F}^{\infty} \frac{1}{2|\varepsilon|}\left[\frac{\phi_\varepsilon}{1+|\varepsilon|} - \Theta(\epsilon_F-\varepsilon)\right]. \tag{57}$$

Equation determining $\phi_\varepsilon \equiv \eta_\varepsilon/\eta_{\varepsilon=0}$ for small temperatures is approximated in our case by:

$$\phi_\varepsilon - \frac{\lambda|\varepsilon|}{2(1+|\varepsilon|)} \int_{\varepsilon'=-\epsilon_F}^{\infty} \frac{\phi_{\varepsilon'}}{(1+|\varepsilon|+|\varepsilon'|)(1+|\varepsilon'|)} = \frac{1}{1+|\varepsilon|}. \tag{58}$$

This is solved iteratively to second order, $\phi_\varepsilon = \phi_\varepsilon^{(0)} + \lambda\phi_\varepsilon^{(1)}$,

$$\phi_\varepsilon = \frac{1}{1+|\varepsilon|} + \lambda\phi_\varepsilon^{(1)}$$

$$\phi_\varepsilon^{(1)} = \frac{1}{2(1+|\varepsilon|)}\left\{\frac{1+2\epsilon_F}{(1+\epsilon_F)} - \frac{1}{|\varepsilon|}\log\frac{(1+|\varepsilon|)^2(1+\epsilon_F)}{1+|\varepsilon|+\epsilon_F}\right\}. \tag{59}$$

Substituting this into Eq. (57) one obtains

$$\zeta(\epsilon_F,\lambda) = \zeta^0(\epsilon_F) + \lambda\zeta^1(\epsilon_F) + O\left(\lambda^2\right)$$

$$\zeta^{(0)}(\epsilon_F) = \int_{\varepsilon=-\epsilon_F}^{\infty} \frac{1}{2|\varepsilon|}\left\{\frac{1}{(1+|\varepsilon|)^2} - \Theta(\epsilon_F-\varepsilon)\right\} = -\frac{1}{2}\left\{\frac{1+2\epsilon_F}{1+\epsilon_F} + \log\left[\epsilon_F(1+\epsilon_F)\right]\right\}. \tag{60}$$

The second correction,

$$\zeta^{(1)}(\epsilon_F) = \int_{\varepsilon=-\epsilon_F}^{\infty} \frac{\phi_\varepsilon^{(1)}}{2|\varepsilon|(1+|\varepsilon|)}, \tag{61}$$

still can be calculated analytically via hypergeometric function but is cumbersome. It is regular and for $\lambda = 0.5$ corrects the analytic result shown in Figs. 4 and 5 as a dotted line into the one (solid line) closer to numerical solution. The formula works better for the nonadiabatic regime, Fig. 5, than in the adiabatic limit, Fig. 4.

The approximate formula neglecting the second-order correction in the adiabatic regime, $\epsilon_F > \Omega$, is

$$T_c = \frac{2}{\pi} e^{\gamma_E} \epsilon_F e^{-\frac{1}{\lambda}} \exp\left[-1 - \log\left[\epsilon_F\right]\right] = \frac{2}{\pi} e^{\gamma_E - 1} \Omega e^{-\frac{1}{\lambda}} \approx 0.41\Omega\, e^{-\frac{1}{\lambda}}. \tag{62}$$

The coefficient is significantly smaller than the fit to the numerical solution, Eq. (46). In the opposite nonadiabatic limit

$$T_c = \frac{2}{\pi} e^{\gamma_E} \epsilon_F e^{-\frac{1}{\lambda}} \exp\left[-\frac{1}{2}\{1 + \log\left[\epsilon_F\right]\}\right] = \frac{2}{\pi} e^{\gamma_E - 1/2} \sqrt{\Omega\epsilon_F} e^{-\frac{1}{\lambda}} \approx 0.69\sqrt{\Omega\epsilon_F} \exp\left[-\frac{1}{\lambda}\right]. \tag{63}$$

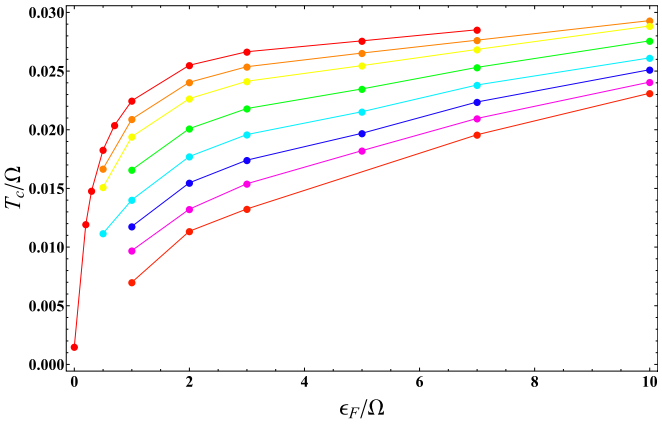

FIG. 6. Suppression of the critical temperature of a 2DEG phonon superconductor the RPA screened Coulomb repulsion. T_c in units of the phonon frequency Ω for $\lambda = 0.32$ is given as a function of the chemical potential for the following dimensionless effective Coulomb repulsion strength α defined in Eq. (64). From top to bottom: $\alpha = 0$ (the phonon model, red dots), $\alpha = 5 \times 10^{-3}$ (brown dots), $\alpha = 10^{-2}$ (yellow), $\alpha = 2 \times 10^{-2}$ (green), $\alpha = 3 \times 10^{-2}$ (blue), $\alpha = 4 \times 10^{-2}$ (violet), $\alpha = 5 \times 10^{-2}$ (pink), and $\alpha = 6 \times 10^{-2}$ (dark red). The curves are well approximated by the interpolating formula, Eqs. (65).

To conclude the critical temperature in the Kirzhnits approach is generally underestimated by 30% in the adiabatic limit and is precise in the nonadiabatic limit. Within the range of applicability the general tendency is correct. Next we tackle a more complicated model incorporating the effect of the screened Coulomb repulsion.

VI. THE EFFECT OF THE COULOMB REPULSION

The eigenvalue equation Eq. (29) with the kernel including the RPA dynamically screened Coulomb repulsion, Eq. (26), is solved numerically by diagonalizing sufficiently large matrix $K_{n_1\varepsilon_1,n_2\varepsilon_2}(T)$. In the presence of moderately screened Coulomb repulsion, to describe the $LaAlO_3$/STO (LaO/STO) interfaces, the chemical potential is practically equal to the Fermi energy ϵ_F.

The integral over the angle ϕ in Eq. (26) was performed numerically (720 subdivisions). The neutralizing background was subtracted (the screening is dynamic, so the interaction is generally still long range, see Appendix B). The Matsubara index is in the range $-N_\omega/2 < n < N_\omega/2$ with the value $N_\omega = 16$ used. The energy cutoff was in the range $\Lambda = 3\epsilon_F$ (for nonadiabatic values $\epsilon_F = 0.5$, 1) and up to $\Lambda = 15\epsilon_F$ in the adiabatic regime. Number of values of energy $N_\varepsilon = 256$, so the step is smaller than $(\epsilon_F + \Lambda)/N_\varepsilon \sim 2.4 \times 10^{-3}$. Convergence was checked against higher values of Λ, N_e, and N_ω.

The critical temperature for given λ, m, ϵ_F, and Ω is determined from the requirement that the largest eigenvalue of $K(T)$ is 1. The use units in which $\hbar = \Omega = m = 1$. In these units the Coulomb couplings become

$$\alpha = \frac{e^2 m^{1/2}}{\epsilon \Omega^{1/2} \hbar}. \tag{64}$$

For $\Omega = 1000$ K, $m = m_e$, $\epsilon = 3000$ one gets $\alpha = 6 \times 10^{-3}$. The results presented in Fig. 6 in the Coulomb coupling range 5×10^{-3}–7×10^{-2} are sufficient for our purposes. One clearly observes the Coulomb suppression that is not homogeneous in ϵ_F. At ϵ_F comparable with Ω or slightly smaller (the smallest simulated value is $\epsilon_F = 0.5\Omega$), one observes that at larger α an approach to the BCS limit is slower.

A reasonable interpolation formula for all the values is

$$T_c(\Omega,\epsilon_F,\lambda) = 0.8\ \Omega \exp\left[-\frac{2}{\lambda - 1.2\alpha}\frac{\Omega + 3\epsilon_F}{\Omega + 6\epsilon_F}\right]. \tag{65}$$

We use this formula to discuss the interface superconductivity in the next section.

VII. APPLICATION TO SUPERCONDUCTIVITY IN 1D FESE/STO SUBSTRATE AND RELATED MATERIALS

A. 1UC FeSe/STO

Based on experiments described in the Introduction, the following parameters should be used in the simple LO model of Sec. IV. The phonon frequency was estimated by ARPES [5] in the $\Omega = 80$–100 meV range and by the ultrafast dynamics [3] to be $\Omega = 106$ meV. The dimensionless electron-phonon coupling constant was estimated (using a model with a flat phonon spectrum) from the intensity ratios in ARPES [5] to be $\lambda = 0.5$, consistent with $\lambda = 0.48$ from the ultrafast dynamics [3]. The critical temperature estimates were rather scattered and dependent on the method. While the critical temperature deduced from the gap in tunneling is $T_c = 70$ K, magnetization experiments [4] indicate that $T_c = 85$ K and the ultrafast[3] dynamics gives $T_c = 68$ K. The temperature was directly measured in transport[2] to be 100 K. The Fermi surface [5] for the electron pockets is located at $\epsilon_F = 60$ meV.

In the simplified model of Sec. II (neglecting completely the Coulomb repulsion due to the huge dielectric constant of STO) the only parameters determining T_c are λ, Ω, and ϵ_F. This is presented in Figs. 2 and 3. Taking $\Omega = 100$ meV, $\epsilon_F = 60$ meV, one obtains, for $\lambda = 0.5$, $T_c = 77$ K, see the dotted line in Figs. 2 and 3. This is within the experimentally possible range. The 2UC FeSe/STO already has three pockets and resembles the parent material more than 1UC FeSe/STO.

B. Interface superconductivity in LAO/STO

In this case the dielectric constant is one order of magnitude smaller ($\epsilon_0 = 186$ on the STO side and $\epsilon_0 = 24$ on the LAO side, see Ref. [18] where accurate electrostatics was considered) than in 1UC FeSe/STO. Consequently, the Coulomb repulsion cannot be neglected, especially in view of very low $T_c \sim 0.2$ K. Therefore we have to use the full model of Sec. IV. In this case one takes $N = 1$ and effective mass $m = 1.65m_e$ (where m_e is the electron mass in a vacuum). Recently [14], the electron-phonon coupling and chemical potential were measured by tunneling from the underdoped to the overdoped region. Generally, in the underdoped region, the chemical potential rises linearly with the gate voltage V_g, $\epsilon_F(V_g) = \mu_0(1 + \eta V_g)$, with the slope $\eta = 1.8 \times 10^{-3}$ V^{-1} and is saturated in the overdoped region at value $\mu_0 = 30$ meV. The electron-phonon coupling apparently decreases very slowly, $\lambda = \lambda_0(1 - \gamma V_g)$, where $\lambda_0 = 0.28$ is the undoped value and $\gamma = 1.1 \times 10^{-4}$ V^{-1} is the slope. Our

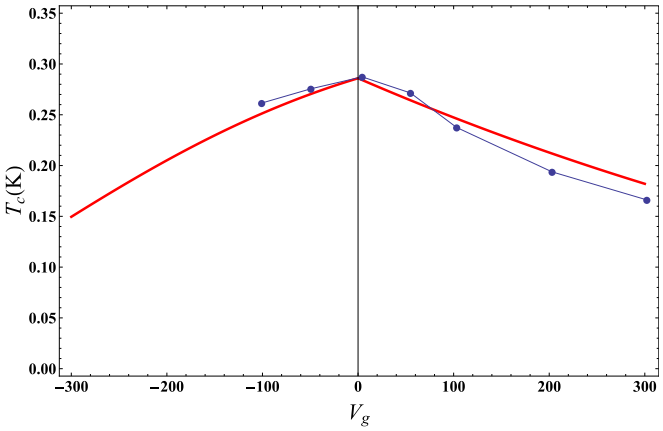

FIG. 7. T_c as a function on gate voltage V_g.

approximate formula Eq. (65) in this case gives the dependence

$$T_c(V_g) = 0.8\,\Omega \exp \times \left[-\frac{2}{\lambda_0(1-\gamma V_g) - 1.2\alpha} \frac{1+3\mu_0(1+\eta V_g)}{1+6\mu_0(1+\eta V_g)} \right]. \quad (66)$$

Taking a measured value for the LO4 mode $\Omega = 99.3$ meV lets us estimate the Coulomb repulsion constant as

$$\alpha = \frac{e^2 m^{1/2}}{\epsilon_{\text{eff}} \Omega^{1/2} \hbar} = 0.09$$

for $\epsilon_{\text{eff}} = 200$. Substituting these values, one obtains the fit to experimental values of Ref. [14], see Fig. 7.

Qualitatively, there are two conflicting tendencies at play. The reduction of the electron-phonon coupling with V_g reduces T_c, while the increase of ϵ_F (the charging appears according to experiment only in the underdoped region) increases T_c. The overall effect is that in the underdoped case the second tendency prevails, while in the overdoped only the first exists. This explains the "dome" shape.

VIII. DISCUSSION AND SUMMARY

Pairing in one atomic layer thick two-dimensional electron gas on a strongly dielectric substrate by a single band of high-energy longitudinal optical phonons is considered in detail. The phonon band is assumed to be nearly dispersionless with frequency Ω. The polar dielectric $SrTiO_3$ exhibits such an energetic phonon mode and the 2DEG is created both when one unit cell FeSe layer is grown on its (100) surface and on the interface with another dielectric like $LaAlO_3$. Both the adiabatic, $\epsilon_F >> \Omega$, and the nonadiabatic, $\epsilon_F << \Omega$, cases are considered and compare well with conventional weak coupling BCS and with the local instantaneous interaction model (describing the nonadiabatic regime close to the BEC crossover [19–22] still assuming that $\epsilon_F >> E_c$, where $2E_c$ is the binding energy, so the pairing is the BCS type rather than BEC), respectively. The focus was, however, on the intermediate region. The reason is that in several novel materials this is precisely the case. In particular, in high T_c one unit cell FeSe on STO the Fermi energy is a bit smaller than the phonon frequency $\epsilon_F = 0.65\Omega$. In interface superconductors like $LaAlO_3$/STO interfaces the ration is smaller $\epsilon_F/\Omega \sim 0.3$ still well above the nonadiabatic limit. It turns out that in the crossover region the critical temperature decreases very slowly as a function of ϵ_F, up to $\epsilon_F = 0.1\Omega$, see Figs. 2 and 3, and only then drops fast to zero.

The critical temperature was calculated within the weak-coupling model of superconductivity. The theory was applied to two different realizations of such a system: 1UC FeSe/STO and $LaAlO_3$/STO interfaces. There is a reduction in the nearly instantaneous electron-electron Coulomb repulsion due to screening by STO, but we believe it is much smaller for the essentially retarded effective electron-electron interaction due to phonons. This reduction due to STO is thus taken into account by the electron-electron interaction. Similarly, we use the "dressed" electron and phonon Green functions with parameters (electron density of states, the phonon frequency). The numerical solution of the gap equation at $\alpha = 0$ was compared with an often-utilized Kirzhnits dielectric approach for arbitrary ratio ϵ_F/Ω. The validity of the Migdal theorem in the nonadiabatic case was not assumed (discussed recently in Ref. [26]). This comparison demonstrated excellent agreement between two theories in the nonadiabatic range while in the adiabatic region the Kirzhnits theory gives lower T_c than the numerical solution of the gap equation.

We conclude that, despite small electron concentration, very high critical temperatures observed recently are consistent with the mostly phononic mechanism already due to combination of two peculiar properties of the system. First, since the optical phonon frequencies Ω are very large and electrons reside in small pockets, Ω is larger than ϵ_F. Second, due to the huge dielectric constant of STO the Coulomb repulsion is strongly suppressed inside the layer leading to small α. The required value of the electron-phonon coupling in the superconducting layer is $\lambda \sim 0.5$ in 1UC FeSe/STO and $\lambda \sim 0.2$ in LAO/STO. In low-T_c LAO/STO the less-suppressed Coulomb repulsion results in significant reduction or even suppression of superconductivity. A phenomenological model for dependence of ϵ_F and λ on electric field for the LAO/STO is proposed.

The main insight from this work therefore is that a small value of ϵ_F is not an obstacle to achieve T_c of order 0.1 Ω as long as λ is sufficiently large and the Coulomb repulsion is effectively suppressed by polarization of the 3D substrate.

Note added. Very recent experiment [27] strengthens the assumptions made in the present work about the nature of superconductivity in 1UC FeSe on STO with measured electron-phonon coupling in the layer as high as $\lambda = 1$.

ACKNOWLEDGMENTS

We are grateful J. Wang, C. Luo, J. J. Lin, M. Lewkowicz, and Y. Dagan for helpful discussions. The work of D.L. and B.R. was supported by NSC of R.O.C. Grant No. 98-2112-M-009-014-MY3 and he MOE ATU program. The work of D.L. was supported by the National Natural Science Foundation of China (Grant No. 11274018).

APPENDIX A: DERIVATION OF THE PAIRING EQUATIONS

We derive the Gorkov equations within the functional approach starting with the effective action [Eq. (16)]. The partition function as a functional of sources $\chi^{\sigma}_{p\omega}$ is

$$Z[\chi] = \int_{\psi} \exp\left[-A_e[\psi] + \int_{p\omega} \left(\psi^{\sigma}_{p\omega}\chi^{*\sigma}_{p\omega} + \chi^{\sigma}_{p\omega}\psi^{*\sigma}_{p\omega}\right)\right]. \tag{A1}$$

The free energy, $\mathcal{F}[\chi] = -\log Z[\chi]$, defines the effective action and the "classical fields" via

$$\mathcal{A}(\psi) = \mathcal{F}[\chi] + \int_{p\omega} \left(\psi^{\sigma}_{p\omega}\chi^{*\sigma}_{p\omega} + \chi^{\sigma}_{p\omega}\psi^{*\sigma}_{p\omega}\right);$$
$$\psi^{\sigma}_{p\omega} = \frac{\delta\mathcal{F}[\chi]}{\delta\chi^{*\sigma}_{p\omega}}, \psi^{*\sigma}_{p\omega} = -\frac{\delta\mathcal{F}[\chi]}{\delta\chi^{\sigma}_{p\omega}}, \tag{A2}$$

where the sources are expressed via the first functional derivative of $\mathcal{A}$,

$$\chi^{\sigma}_{p\omega} = -\frac{\delta\mathcal{A}[\psi]}{\delta\psi^{*\sigma}_{p\omega}}, \chi^{*\sigma}_{p\omega} = \frac{\delta\mathcal{A}[\psi]}{\delta\psi^{\sigma}_{p\omega}}. \tag{A3}$$

The inverse propagators, the second derivatives, form a Nambu matrix:

$$\Gamma^{\sigma\rho}_{p\omega q\nu} = \frac{\delta^2\mathcal{A}}{\delta\psi^{\rho}_{q\nu}\delta\psi^{\sigma}_{p\omega}}; \Gamma^{\sigma\rho}_{p\omega q\nu} = \frac{\delta^2\mathcal{A}}{\delta\psi^{\rho}_{q\nu}\delta\psi^{\sigma}_{p\omega}};$$
$$\Gamma^{\sigma*\rho}_{p\omega q\nu} = \frac{\delta^2\mathcal{A}}{\delta\psi^{\rho}_{q\nu}\delta\psi^{\sigma*}_{p\omega}}. \tag{A4}$$

Green's functions also form a Nambu matrix,

$$G^{\rho\sigma}_{q\nu p\omega} = \left\langle\psi^{\sigma*}_{p\omega}\psi^{\rho}_{q\nu}\right\rangle = -\frac{\delta^2\mathcal{F}}{\delta\chi^{\rho*}_{q\nu}\delta\chi^{\sigma*}_{p\omega}};$$
$$G^{\rho*\sigma*}_{q\nu p\omega} = -\frac{\delta^2\mathcal{F}}{\delta\chi^{\rho}_{q\nu}\delta\chi^{\sigma}_{\omega}};$$
$$G^{\rho\sigma*}_{q\nu p\omega} = \left\langle\psi^{\sigma}_{p\omega}\psi^{\rho}_{q\nu}\right\rangle = -\frac{\delta^2\mathcal{F}}{\delta\chi^{\rho*}_{q\nu}\delta\chi^{\sigma}_{p\omega}}. \tag{A5}$$

The two Nambu matrices obey $\Gamma^{AC}G^{CB} = \delta^{AB}$, which constitute the Gorkov equations.

Let us now calculate Γ. The Gaussian average first derivatives, assuming only anomalous averages, are

$$\chi^{\sigma}_{p\omega} = D^{-1}_{p\omega}\psi^{\sigma}_{p\omega} - V_{p-p_2,\omega-\omega_2}\psi^{\kappa*}_{p_3\omega_3}\left\langle\psi^{\sigma}_{p_2\omega_2}\psi^{\kappa}_{p-p_2+p_3,\ \omega-\omega_2+\omega_3}\right\rangle. \tag{A6}$$

The second derivatives are

$$\Gamma^{\sigma*\rho}_{p\omega q\nu} = \delta^{\sigma\rho}\delta^{\omega\nu}\delta_{pq}D^{-1}_{p\omega};$$
$$\Gamma^{\sigma\rho}_{p\omega q\nu} = V_{q-p_2,\omega-\omega_1}\delta_{-p_1-p_2+q+p}\delta_{\omega-\omega_1-\omega_2+\nu}\left\langle\psi^{\sigma*}_{p_1\omega_1}\psi^{\rho*}_{p_2\omega_2}\right\rangle. \tag{A7}$$

Using the translation symmetry,

$$\left\langle\psi^{1}_{p\omega}\psi^{2}_{q\nu}\right\rangle = \delta_{\omega+\nu}\delta_{p+q}F_{p\omega},$$
$$\Gamma^{\sigma\rho}_{p\omega q\nu} = \left\langle\psi^{1*}_{p\omega}\psi^{2}_{q\nu}\right\rangle = \delta^{\sigma\rho}\delta_{p+q}\delta_{\omega+\nu}D^{-1}_{p\omega}, \tag{A8}$$

the equation $\Gamma^{AC}G^{CB} = \delta^{AB}$ becomes Eqs. (19) and (20).

APPENDIX B: LONG-RANGE RPA SCREENED COULOMB REPULSION

In Eq. (26) one detail was not presented: subtraction of the neutralizing background. Since at nonzero frequency the screened repulsion does not become short ranged, the neutralizing background should be taken into account. For our purposes the jellium model suffices [23]. To this end, one needs the infrared cutoff L. The results for sufficiently large L converge (numerical simulations were performed for $L = 30\frac{\Lambda+\epsilon_F}{N_\varepsilon-1}$).

The electronic part of the kernel Eq. (26), in our units of $\hbar = m = \Omega$ (unit of length $\hbar/\sqrt{\Omega m}$), is

$$P^{\mathrm{RPA}}_{\mathbf{p},\mathbf{k},\omega} = \frac{e^2}{\epsilon}\left\{\frac{\epsilon|\mathbf{p}-\mathbf{k}|}{2\pi e^2} + \frac{1}{\pi}\left(1 - \frac{|\omega|}{\sqrt{\omega^2 + v_F^2|\mathbf{p}-\mathbf{k}|^2}}\right)\right\}^{-1} - \frac{2\pi e^2}{\epsilon L}\delta(\boldsymbol{p}-\boldsymbol{k}), \tag{B1}$$

transformed to polar coordinates (using the rotation invariance) and then changing to the energy variable $\varepsilon_p = p^2/2 - \epsilon_F$ results in

$$P^{\mathrm{RPA}}_{\varepsilon_1,\varepsilon_2,n} = \frac{e^2}{\epsilon}\int_{\phi=0}^{2\pi}\frac{1}{A+2B} - \frac{2e^2}{\epsilon L}\delta(\varepsilon_1-\varepsilon_2); \tag{B2}$$
$$A = \frac{\epsilon}{e^2}\left\{\sqrt{2[\varepsilon_1+\varepsilon_2+2\epsilon_F - 2\sqrt{(\varepsilon_1+\epsilon_F)(\varepsilon_2+\epsilon_F)}\cos\phi]} + \frac{\pi}{L}\right\};$$
$$B = 1 - \frac{|\omega-\nu|}{\sqrt{\omega_n^2 + 4\mu[\varepsilon_1+\varepsilon_2+2\epsilon_F - 2\sqrt{(\varepsilon_1+\epsilon_F)(\varepsilon_2+\epsilon_F)}\cos\phi]}}.$$

[1] Q.-Y. Wang, Z. Li, W.-H. Zhang, Z.-C. Zhang, J.-S. Zhang, W. Li, H. Ding, Y. B. Ou, P. Deng, K. Chang, J. Wen, C.-L. Song, J.-F. Jia, S.-H. Ji, Y.-Y. Wang, Xi Chen, X.-C. Ma, and Qi-K. Xue, Chin. Phys. Lett. **29**, 037402 (2012); D. Liu, W. Zhang, D. Mou, J. He, Y.-Bo Ou, Q.-Y. Wang, Z. Li, L. Wang, L. Zhao, S. He, Y. Peng, Xu Liu, C. Chen, Li Yu, G. Liu, X. Dong, Jun

Zhang, C. Chen, Z. Xu, J. Hu, Xi Chen, X. Ma, Q. Xue, and X. J. Zhou, Nat. Commun. **3**, 931 (2012); S. He, J. He, W. Zhang, L. Zhao, D. Liu, Xu Liu, D. Mou, Yun-Bo Ou, Q.-Y. Wang, Z. Li, L. Wang, Y. Peng, Yan Liu, C. Chen, Li Yu, G. Liu, X. Dong, Jun Zhang, C. Chen, Z. Xu, Xi Chen, X. Ma, Q. Xue, and X. J. Zhou, Nature Mater. **12**, 605 (2013); S. Tan, Yan Zhang, M. Xia, Z. Ye, Fei Chen, Xin Xie, Rui Peng, D. Xu, Q. Fan, H. Xu, J. Jiang, T. Zhang, X. Lai, T. Xiang, J. Hu, B. Xie, and D. Feng, Nat. Mater. **12**, 634 (2013); W.-H. Zhang, Yi. Sun, J.-S. Zhang, F.-S. Li, M.-H. Guo, Y.-F. Zhao, H.-M. Zhang, J.-P. Peng, Ying Xing, Hui-Chao Wang, T. Fujita, A. Hirata, Zhi Li, Hao Ding, C.-J. Tang, Meng Wang, Q.-Y. Wang, Ke He, S.-H. Ji, Xi Chen, J.-F. Wang, Z.-C. Xia, Liang Li, Ya-Yu Wang, Jian Wang, and Li-Li Wang, Chin. Phys. Lett. **31**, 017401 (2014); Qingyan Wang, Wenhao Zhang, Zuocheng Zhang, Yi Sun, Ying Xing, Yayu Wang, Lili Wang, Xucun Ma, Qi-Kun Xue, and Jian Wang, 2D Mater. **2**, 044012 (2015).

[2] J.-F. Ge, Z.-L. Liu, C. Liu, C.-L. Gao, D. Qian, Qi-Kun Xue, Y. Liu, and J.-F. Jia, Nat. Mater. **14**, 285 (2015).

[3] Y. C. Tian, W. H. Zhang, F. S. Li, Y. L. Wu, Q. Wu, F. Sun, Lili Wang, X. Ma, Qi-K. Xue, and J. Zhao, Phys. Rev. Lett. **116**, 107001 (2016).

[4] Yi Sun, W. Zhang, Ying Ding, F. Li, Y. Zhao, Z. Xia, Lili Wang, X. Ma, Qi-Kun Xue, and Jian Wang, Sci. Rep., **4**, 6040 (2014); L. Z. Deng, B. Lv, Z. Wu, Y. Y. Xue, W. H. Zhang, F. S. Li, L. L. Wang, X. C. Ma, Q. K. Xue, and C. W. Chu, Phys. Rev. B **90**, 214513 (2014).

[5] J. J. Lee, F. T. Schmitt, R. G. Moore, S. Johnston, Y.-T. Cui, W. Li, M. Yi, Z. K. Liu, M. Hashimoto, Y. Zhang, D. H. Lu, T. P. Devereaux, D.-H. Lee, and Z.-X. Shen, Nature **515**, 245 (2014).

[6] Q. Fan, W. H. Zhang, X. Liu, Y. J. Yan, M. Q. Ren, R. Peng, H. C. Xu, B. P. Xie, J. P. Hu, T. Zhang, and D. L. Feng, Nat. Phys., **11**, 946 (2015); C. Tang, C. Liu, G. Zhou, F. Li, H. Ding, Z. Li, D. Zhang, Z. Li, C. Song, S. Ji, K. He, L. Wang, X. Ma, and Q.-K. Xue, Phys. Rev. B **93**, 020507 (2016).

[7] F.-C. Hsu, J.-Y. Luo, K.-W. Yeh, Ta-Kun Chen, T.-W. Huang, P. M. Wu, Y.-C. Lee, Yi-Lin Huang, Yan-Yi Chu, D.-C. Yan, and M.-K. Wu, Proc. Natl. Acad. Sci. USA **105**, 14262 (2008).

[8] N. Choudhury, E. J. Walter, A. I. Kolesnikov, and C.-K. Loong, Phys. Rev. B **77**, 134111 (2008); W. G. Stirling, J. Phys. C **5**, 2711 (1972).

[9] P. J. Hirschfeld, C. R. Physique **17**, 197 (2016).

[10] Y. Y. Xiang, F. Wang, D. Wang, Q. H. Wang, and D. H. Lee, Phys. Rev. B **86**, 134508 (2012).

[11] X. Chen, S. Maiti, A. Linscheid, and P. J. Hirschfeld, Phys. Rev. B **92**, 224514 (2015).

[12] L. P. Gorkov, Phys. Rev. B **93**, 060507(R) (2016).

[13] N. Reyren, S. Thiel, A. Caviglia, L. F. Kourkoutis, G. Hammerl, C. Richter, C. Schneider, T. Kopp, A.-S. Ruetschi, D. Jaccard, M. Gabay, D. Muller, J.-M. Triscone, and J. Mannhart, Science **317**, 1196 (2007); A. Caviglia, S. Gariglio, N. Reyren, D. Jaccard, T. Schneider, M. Gabay, S. Thiel, G. Hammerl, J. Mannhart, and J.-M. Triscone, Nature **456**, 624 (2008); C. Richter, H. Boschker, W. Dietsche, E. Fillis-Tsirakis, R. Jany, F. Loder, L. F. Kourkoutis, D. A. Muller, J. R. Kirtley, C. W. Schneider, and J. Mannhart, *ibid.* **502**, 528 (2013); N. Reyren, S. Gariglio, A. D. Caviglia, D. Jaccard, T. Schneider, and J.-M. Triscone, Appl. Phys. Lett. **94**, 112506 (2009); T. Schneider, A. D. Caviglia, S. Gariglio, N. Reyren, and J.-M. Triscone, Phys. Rev. B **79**, 184502 (2009); E. Maniv, M. Ben Shalom, A. Ron, M. Mograbi, A. Palevski, M. Goldstein, and Y. Dagan, Nat. Commun. **6**, 8239 (2015).

[14] H. Boschker, C. Richter, E. Fillis-Tsirakis, C. W. Schneider, and J. Mannhart, Sci. Rep. **5**, 12309 (2015).

[15] S. N. Klimin, J. Tempere, J. T. Devreese, and D. van der Marel, Phys. Rev. B **89**, 184514 (2014).

[16] D. A. Kirzhnits, E. G. Maksimov, and D. I. Khomskii, J. Low Temp. Phys. **10**, 79 (1973).

[17] Y. Takada, J. Phys. Soc. Jpn. **45**, 786 (1978); **49**, 1267 (1980); **49**, 1713 (1980).

[18] S. N. Klimin, J. Tempere, D. van der Marel, and J. T. Devreese, Phys. Rev. B **86**, 045113 (2012); J. L. M. van Mechelen, D. van der Marel, C. Grimaldi, A. B. Kuzmenko, N. P. Armitage, N. Reyren, H. Hagemann, and I. I. Mazin, Phys. Rev. Lett. **100**, 226403 (2008); J. T. Devreese, S. N. Klimin, J. L. M. van Mechelen, and D. van der Marel, Phys. Rev. B **81**, 125119 (2010).

[19] J. Levinsen, M. M. Parishyar, Strongly interacting two-dimensional Fermi gases, in *Annual Review of Cold Atoms and Molecules*, Vol. 3, edited by Kirk W. Madison, Kai Bongs, Lincoln D. Carr, Ana Maria Rey, and Hui Zhai (World Scientific Publishing, Singapore, 2015).

[20] L. P. Gor'kov and T. K. Melik-Barkhudarov, Sov. Phys. JETP **13**, 1018 (1961); J. Expt. Theoret. Phys. (U.S.S.R.) **40**, 1452 (1961); H. Heiselberg, C. J. Pethick, H. Smith, and L. Viverit, Phys. Rev. Lett. **85**, 2418 (2000); R. Haussmann, *Self-Consistent Quantum-Field Theory and Bosonization for Strongly Correlated Electron Systems* (Springer Science and Business Media, 2003).

[21] M. Randeria and J.-M. Duan, and L.- Y. Shieh, Phys. Rev. Lett. **62**, 981 (1989)

[22] A. V Chubukov, I. Eremin, D. V. Efremov, Phys. Rev. B **93**, 174516 (2016)

[23] A. L. Fetter, and J. D. Valecka, *Quantum Theory of Manybody Systems* (McGraw-Hill, New York, 1971).

[24] L. P. Gorkov, Phys. Rev. B **93**, 054517 (2016).

[25] D. N. Zubarev, Sov. Phys. Usp. **3**, 320 (1960).

[26] B. Roy, J. D. Sau, and S. Das Sarma, Phys. Rev. B **89**, 165119 (2014); Y. Wang, K. Nakatsukasa, L. Rademaker, T. Berlijn, and S. Johnston, Supercond. Sci. Technol. **29**, 054009 (2016).

[27] S. Zhang, J. Guan, X. Jia, B. Liu, W. Wang, F. Li, L. Wang, X. Ma, Q. Xue, J. Zhang, E. W. Plummer, X. Zhu, and J. Guo, The Role of SrTiO3 Phonon Penetrating into thin FeSe Films in the Enhancement of Superconductivity, arXiv:1605.06941v1 [cond-mat.supr-con] (2016).